Furfural production in a biphasic system using a carbonaceous solid acid catalyst

Gerardo Gomez Millan,[a,b] Josphat Phiri, [a] Mikko Mäkelä,[a] Thad Maloney, [a] Alina M. Balu,[c] Antonio Pineda,[c] Jordi Llorca,[b] Herbert Sixta[a]*

[a] Department of Bioproducts and Biosystems
School of Chemical Engineering, Aalto University
Vuorimiehentie 1, 02150 Espoo (Finland)
E-mail: herbert.sixta@aalto.fi
[b] Department of Chemical Engineering, Institute of Energy Technologies and
Barcelona Research Center in Multiscale Science and Engineering
Universitat Politècnica de Catalunya
Eduard Maristany 10-14, 08019 Barcelona (Spain)
[c] Departmento de Química Orgánica
Universidad de Cordoba
Campus Rabanales, Edificio Marie Curie (C-3)
Ctra Nnal IV-A, km 396 Cordoba (Spain)

Abstract

The formation of furfural from xylose was investigated under heterogeneously catalyzed conditions with sulfonated Starbon®450-SO_3H as catalyst in a biphasic system. Experiments were performed based on a statistical experimental design. The variables considered were time, temperature and the ratio of aqueous to organic phase. The results indicate that sulfonated Starbon®450-SO_3H can be an effective solid acid catalyst for furfural formation. Starbon®450-SO_3H was characterised by scanning electron microscopy, N_2-physisorption, thermogravimetric analysis, diffuse reflectance infrared Fourier transform, Raman spectroscopy, pyridine titration and X-ray photoelectron spectroscopy. A maximum furfural yield and selectivity of 70 mol% was achieved at complete xylose conversion under optimum experimental conditions. The present paper suggests that functionalized Starbon®450-SO_3H can be employed as an efficient solid acid catalyst that has significant hydrothermal stability and can be reused for several cycles to produce furfural from xylose.

Keywords: xylose, furfural, starbon, CPME, heterogeneous catalysis, biorefinery

Introduction

Furfural (FUR) has been highlighted as one of the top ten most rewarding bio-based building blocks by the United States Department of Energy. FUR can be employed directly as a chemical solvent and selective extractant, fungicide and as a component of disinfectors, rust removers and pesticides.[1, 2] Furthermore, FUR withholds the potential to be further transformed directly or indirectly into more than 80 valuable chemicals[2]. Among these chemicals, FUR can be hydrogenated to furfuryl alcohol, which has applications in the biofuel and food industries (furfuryl alcohol represents around 60% of the FUR market[3]). It can also be used in the manufacturing of chemical resistant furanic resins. Other attractive chemicals that can be obtained from FUR are levulinic acid, 2-methyltetrahydrofuran, furan and furoic acid.[2, 4]

FUR is typically produced by dehydration of C_5-sugars (arabinose and xylose) contained in the hemicellulose of lignocellulosic biomass. The production of FUR at industrial scale is associated with high reaction temperatures (approximately 200 °C) and mineral acids (usually sulfuric and hydrochloric acids) that have various process drawbacks, such as the production of toxic effluents, equipment corrosion and consumption of high stripping-steam-to-FUR ratios. Furthermore, the number of side reactions under these conditions limits FUR yields to approximately 50%.[5] Recent research in this field has focused on increasing the FUR yield with reusable solid acid catalysts to replace typically used homogenous acid catalyzed conditions. A wide range of solid acid catalysts for this purpose have been developed to produce FUR from xylose, such as zirconia,[6-9]alumina,[9, 10] zeolites,[9, 11-16] aluminosilicates supported with metals,[17] modified silica,[18-25] sulfonated graphenes,[26] heteropolyacids,[7, 27, 28] coated activated carbon,[29] and resins.[21, 30, 31] However, one of the main challenges of heterogeneous catalysis is the hydrothermal stability of the solid catalysts and the blocking of active sites by humins (insoluble polymeric products formed via condensation and resinification of furanic compounds).[6, 15, 32]

Carbon-based catalysts offer high hydrothermal stability.[33] Carbon materials, such as functionalized activated carbon,[29] offer exciting opportunities for the catalytic conversion of

biomass into value-added chemicals due to their potential to be produced from biomass, their ability to be functionalized by various methods and their hydrothermal stability. Sairanen et al[29] impregnated activated carbon with H_2SO_4, HNO_3 and a combination of both in order to form FUR from xylose in aqueous media. Even though xylose conversion is complete under the reported experimental conditions, FUR yield is not shown in the paper and the reusability of the catalyst is not mentioned. In a similar way, Termvidchakorn et al[34] functionalized multi-wall carbon nanotubes with mineral and organic acids. They employed the functionalized catalysts to form FUR from xylose and achieved the highest xylose conversion (95%) when adding Co ($Co(NO_3)_2 \cdot 6H_2O$ was used as precursor) in 3 h at 170 °C. Nevertheless, the amount of FUR yield was not reported. Moreover, the carbon-based catalysts employed were not investigated for their hydrothermal stability or reusability potential. Unlike previous carbon-based catalysts, Lam et al[26] developed a sulfonated graphene oxide that yielded FUR (62%) in 35 min at 200 °C in water. Nevertheless, the production of graphene oxide includes several steps and various chemicals. Jalili et al. reported in their recent paper that graphene derivatives contain silicon, which has a significant impact on their performance.[35] Among these carbon-based catalysts, a mesoporous material derived from renewable bio-resources (potato and corn starches) known as Starbon®450-SO_3H has demonstrated superior selectivities and activities in various acid catalyzed aqueous phase reactions, such as the esterification of succinic acid.[36-39] In addition, Starbon®450-SO_3H functionalities can be tuned, such as hydrophilicity, which makes it possible to dehydrate xylose in an aqueous phase.

The aim of the present paper was to employ Starbon®450-SO_3H as a solid acid catalyst for the dehydration of xylose to produce FUR. Cyclopentyl methyl ether (CPME) was added to the aqueous xylose solution to extract formed FUR into the organic phase as part of a biphasic system.[40] CPME has demonstrated to be an efficient green solvent in the extraction of FUR.[41, 42] Furthermore, the hydrothermal stability of the solid acid catalyst and its reusability were

thoroughly investigated. The characteristics of the solid catalyst were studied in detail by SEM, EDX, N_2-physorption, Py-titration, TGA, DRIFT and Raman spectroscopy.

Experimental

Materials

D-Xylose powder (99%, Sigma Aldrich), CPME (99.9%, Sigma Aldrich) furfural (99%, Sigma Aldrich), potato starch (Sigma Aldrich), sulfuric acid (49–51%, HPLC grade, Sigma Aldrich) were used in the experiments and as calibration standards as purchased, without further purification. Formic acid (98%, Sigma Aldrich), levulinic acid (99%, Sigma Aldrich) and acetic acid (99%, HPLC grade, Sigma Aldrich) were used for the preparation of calibration standards for HPLC analysis. Millipore grade water was used for preparing the solutions.

Methods

Xylose Dehydration Reaction Experiments in Biphasic System

D-xylose in a concentration typical for biomass hydrolysate (186 mmol l^{-1}) was freshly prepared before the experiments. These experiments were performed in auto-catalyzed reaction system where some side products (namely carboxylic acids) or intermediates, formed during the reaction, may have had a catalytic effect.[43, 44] In a typical experiment, the samples were prepared by heating 0.75 ml of an aqueous solution of 186 mmol l^{-1} xylose, 2.25 ml of CPME and 21 mg of sulfonated Starbon®450-SO_3H using a glass reactor (V = 8 cm^3) with magnetic stirring (600 min^{-1}) (Figure S1, Tables S1 and S2 in the Supplementary Information). The vials were heated up in a silicone oil bath until the desired temperature was reached. Time zero was set when the vials were immersed into the oil bath. Towards the reaction end time, the vials were pulled up from the silicone oil bath and rapidly cooled in an ice bath. The prepared solutions were used for determining FUR yield, selectivity and xylose conversion in different reaction conditions. After reaction, vials were rapidly cooled by submerging them into an ice bath. The individual

experiments were organized according to a central composite design on two variables. This design enabled to determine the effects and statistical significance of the reaction conditions on sample properties. The variables, reaction temperature and time, were varied on three different levels. The design thus consisted of 11 experiments, including 3 replicated experiments at the design center (175 °C in 12.5 h) (Table 1).

Determination of FUR and by-products

Samples for analysis were drawn from both the organic phase (top) and the aqueous phase (bottom) after microwave heating. Xylose, carboxylic acids (formic, acetic and levulinic acids) and FUR from aqueous phase were analyzed separately by High Performance Liquid Chromatography (HPLC) operating a Dionex UltiMate 3000 HPLC (Dionex, Sunnyvale, CA, USA) device equipped with refractive index (RI) and ultraviolet (UV) diode array detectors. Product separation was achieved on a Rezex ROA-Organic Acid H^+ (8%) LC column (7.8 mm × 300 mm, Phenomenex, USA). Aqueous sulfuric acid (0.0025 mol l^{-1}) was used as eluent with a flow rate of 0.5 ml min^{-1}. The column temperature and the RI-detector temperature were set to 55 °C. The FUR concentration was determined by the UV-detector at a wavelength of 280 nm. Xylose concentration was simultaneously analyzed by the RI-detector and the UV-detector at 210 nm.[45] The samples were filtered through a 0.45 μm syringe filter before the analysis.

FUR from the organic phase was analyzed by gas chromatography with a flame ionization detector (GC-FID) relative to iso-butanol as internal standard (IS). The column used was a DB-WAXetr (30 m, 0.32 mm i.d., 1 μm film thickness) from Agilent Technologies Inc. The injected samples (0.5 μL) were subjected to a splitless ratio of 20:1 in the inlet, which was maintained at 250 °C and pressure of 13 psi. Helium was used as the carrier gas. The oven was initially maintained at 80 °C for 1 min, after which the temperature was increased to 250 °C at 30 °C min^{-1}.

The FID was operated at 250 °C with hydrogen, air, and helium delivered at 30 mL min^{-1}, 380 ml min^{-1}, and 29 ml min^{-1}, respectively.

Catalyst preparation

Starbon®450-SO_3H catalyst was synthesized according to known literature procedure with minor modifications.[46] First, the starting material (starch from potato, Sigma-Aldrich) was heated up in water to 140 °C for 2 h (150 g starch in 3 L deionized water). Upon cooling the warm solution was poured into a vial at room temperature, and it was further cooled down to 5 °C for 48 h until formation of a porous gel in water. To avoid the structure to collapse while drying, several solvent exchange steps were conducted until water was fully replaced by ethanol (5 times), and finally by acetone (2 times) to stabilize the porous network. The resulting materials were then filtered off and dried overnight at 50 °C under vacuum, rendering the mesoporous starch structure, subsequently calcined at 450 °C under inert atmosphere (N_2, 50 mL min^{-1}) by using the following heating conditions: from RT to 450 °C, heating rate 1 °C min^{-1}; temperature maintained for 1 h. A purge with nitrogen prior to carbonization was conducted to ensure the absence of oxygen in the first steps of carbonization.

For sulfonation, the calcined Starbon®450 material was suspended in H_2SO_4 of 95-97% purity (10 mL acid per gram of material and 4 h at 80 °C). After sulfonation, samples were thoroughly washed with distilled water until neutral pH value, and finally oven dried at 100 °C overnight. The resulting functionalized mesoporous acid material is denoted as Starbon®450-SO_3H (STARch carBONized at 450 °C with sulfonic acid groups).

Catalyst characterization

Scanning electron microscopy (SEM) images were recorded at 5 kV using a JEOL JSM-7800F PRIME Schottky Field Emission Scanning Electron Microscope equipped with a high resolution Gentle Beam (GBSH). Samples were deposited on conductive carbon tabs. The instrument has

a field emission gun and it is also equipped with an EDX (energy dispersive X-ray) detector for chemical analysis.

Thermogravimetric analysis (TGA) was carried out in a Setaram Setsys 12 using air as carrier gas (50 mL min^{-1}). The sample was loaded in ceramic crucibles with α-Al_2O_3 used to as reference compound and a Pt/Pt-Rh (10%) thermocouple. The heating rate employed was 10 K min^{-1} in all cases.

Diffuse Reflectance Infrared Fourier Transform (DRIFT) spectra were recorded on an ABB BOMEM MB 3000 Instrument equipped with an environmental chamber (Spectra Tech, P/N, 0030-100) placed in the diffuse reflectance attachment. The resolution was 8 cm^{-1} and 256 scans were averaged to obtain the spectra in the 4000-400 cm^{-1} range. Spectra were recorded by using KBr as a reference. The samples for DRIFTS studies were prepared by mechanically grinding all reactants to a fine powder (sample/KBr 1:5.7 ratio).

A Micromeritics Tristar II-Physisorption Analyzer was utilized to record the nitrogen sorption isotherms for fresh and spent catalysts. All samples were dried at 105 °C and exposed to nitrogen gas for 12 h before measurement and the isotherms were taken at 77 K. The samples were exposed to ~20 % humid room air for about 1 minute during the transfer to the holders. The specific surface area (A_{BET}) was determined by the Brunauer-Emmett-Teller (BET) model[47] at relative pressures between 5 and 35% where the data points were observed to arrange linearly. The specific pore volume (V_p) was estimated from N_2 uptake at a p/p_0 value of 0.99 while recording approximately 150 equilibrium data points. The pore width distribution (d_p) was deduced from the desorption branch using the Barrett-Joyner-Halenda (BJH) method.[48]

Xylose adsorption tests were done by stirring 3 mL of an aqueous solution of 186 mmol l^{-1} xylose using a borosilicate glass reactor (V = 10 cm^3) with magnetic stirring (600 min^{-1}) and 50 mg of

Starbon®450-SO_3H. Agitation of the suspension for 24 h at room temperature (25 °C). Determination of xylose adsorption was performed by HPLC analysis.

Pyridine (PY) titration experiments were conducted similarly to the method found in the literature with few modifications.[49] The experiments were performed at 200 °C via gas phase adsorption of the basic probe molecules utilising a pulse chromatographic titration methodology. Briefly, probe molecules (typically 2-5 μL) were injected into a gas chromatograph (GC) through a microreactor in which the solid acid catalyst was previously placed. Basic compounds were adsorbed to full saturation, from where the peaks of the probe molecules in the gas phase were detected in the GC. The quantity of probe molecule adsorbed by the solid acid catalyst could subsequently be easily quantified.

Raman spectra were measured using a WITec alpha300 R Raman microscope (alpha 300, WITec, Ulm, Germany) equipped with a piezoelectric scanner using a 532 nm linear polarized excitation laser. The measurement was conducted directly on the powder catalyst after washing and drying.

The surface characterization was done with X-ray photoelectron spectroscopy (XPS) on a SPECS system equipped with an Al anode XR50 source operating at 150 mW and a Phoibos 150 MCD-9 detector. The pressure in the analysis chamber was always below 10^{-7} Pa. The area analyzed was about 2 mm × 2 mm. The pass energy of the hemispherical analyzer was set at 25 eV and the energy step was set at 0.1 eV. The sample powders were pressed to self-consistent disks for XPS analysis.

In this study conversion was defined in terms of moles of reactant converted per unit volume of reactor (Eq. 1). Selectivity, at an instant, was the generated number of moles of desired product referred to the moles of reactant converted (Eq. 2). Yield was calculated as the amount in moles of desired product (FUR) produced related to the amount of xylose converted (Eq. 3)[50]. The following equations were used for deriving these parameters:

$$X_{xyl} = \frac{c_{xyl}^{in} - c_{xyl}^{f}}{c_{xyl}^{in}} \times 100\ [\%] \qquad \text{(Eq. 1)},$$

$$Y_{fur} = \frac{c_{fur}}{c_{xyl}} \times 100\ [\%] \qquad \text{(Eq. 2)},$$

$$S_{xyl}^{fur} = \frac{c_{fur}}{c_{xyl}^{in} - c_{xyl}^{f}} \times 100\ [\%] \qquad \text{(Eq. 3)},$$

where X, S, Y are the– conversion of xylose, selectivity to FUR and FUR yield, respectively; *c* is the– concentration in mmol l^{-1} (the subscripts *xyl*, *fur*, *in*, *f* refer to xylose, FUR, initial, final). The original experimental design and the calculated results are illustrated in Table 1.

Table 1. Variables and the calculated response values based on the experiments.

Exp. No	T (°C)	t (h)	Furfural Yield (%)	Xylose Conversion (%)	Selectivity (%)
1	150	1	0.7	1.3	53.1
2	200	1	69.5	95.9	72.5
3	150	24	52.2	79.5	65.6
4	200	24	21	100	21.0
5	150	12.5	54.4	78.5	69.2
6	200	12.5	50.3	100	50.3
7	175	1	20	30.8	64.8
8	175	24	60.2	100	60.2
9	175	12.5	61.8	100	61.8
10	175	12.5	63.2	100	63.2
11	175	12.5	64.6	100	64.6

Once the concentrations of FUR and xylose had been determined in each sample, individual prediction models were built for xylose conversion, furfural yield and selectivity separately by solving the general linear regression equation (Eq. 4).[51]

$$y = Xb + e \qquad \text{(Eq. 4)}$$

by minimizing the sum of squares of model residuals through the least-squares estimate (Eq. 5):

$$b = (X^T X)^{-1} X^T y \qquad \text{(Eq. 5)}$$

where *y* denoted a vector of response values, *X* the mean-centered and coded design matrix including interaction and second-order terms, *b* a vector of model coefficients and *e* the model residuals. Statistically insignificant model terms ($p > 0.10$) were excluded based on an F-test that compared the effects with the respective model residuals. The performance of the models was expressed through the R^2 value, which indicated the proportion of data variation explained by each individual model.

Results and Discussion

Catalyst characterization

SEM/EDX

Fig. 3 corresponds to a representative image of Starbon®450-SO_3H catalyst powder revealing the characteristic morphology of particles with sharp edges similar to that reported in the literature.[52] Particles are compact and their size is in the range of 50-100 μm.

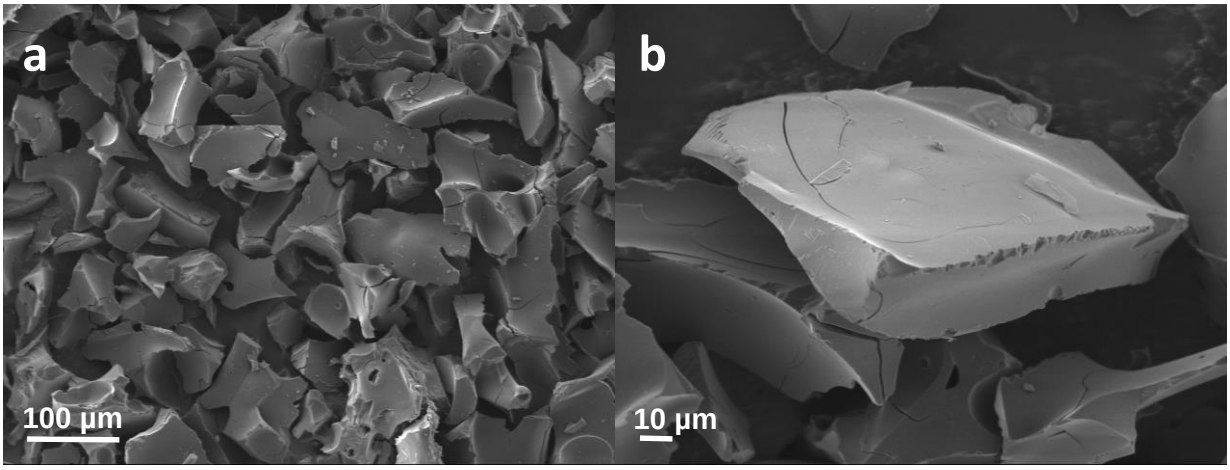

Figure 3. SEM images of the Starbon®450-SO_3H catalyst powder obtained at different magnifications, (a) 180X and (b) 650X.

EDX analyses showed that the catalyst had a very homogeneous composition. Table 1 compiles the mean values obtained in three different regions of the sample. They showed small variations in the content of the elements detected (0.2%).

Table 1. Energy-dispersive X-ray spectroscopy (EDX) analysis of Starbon®450-SO_3H.

Element	Wt. %	Atomic %
C	68.9 ± 0.2	75.2 ± 0.2
O	29.3 ± 0.2	24.0 ± 0.2
S	1.8 ± 0.1	0.8 ± 0.0
Total:	100.0	100.0

DRIFT and thermal gravimetric analysis

The DRIFT spectra of Starbon®450-SO_3H is shown in Figure 4. It exhibits two maxima at 1735 cm^{-1} and 1612 cm^{-1}, which can be assigned to asymmetric stretching vibrations of –COOH carboxyl and $–COO^-$ carbonyl and/or –C=O ketone units and to the stretching vibrations of C=C bonds in aromatic carbon rings, respectively.[53] The band at 1227 cm^{-1} can be attributed to asymmetric stretch of –C-C-C bridges in ketonic groups and/or to deformation vibrations of O-H in the carboxylic acid groups. XPS spectra exhibits a peak at 1057 cm^{-1}, which is assigned to symmetric S=O stretching of sulfonic groups attached to the material.[54-57] [58] In order to study

the pyrolysis process and how the rate of heating affects the material during the pyrolytic formation of Starbon®450-SO_3H, DTA/TGA curves were recorded (Figure S4). The DTA curve for Starbon®450-SO_3H exhibits two exothermic peaks at 100 °C and 540 °C due to moisture in the sample and to the combustion of the carbon matrix, respectively.[40] The TGA curve of Starbon®450-SO_3H showed a steep weight loss of nearly 70% between 350 °C and 600 °C due to the combustion of the carbonaceous material.

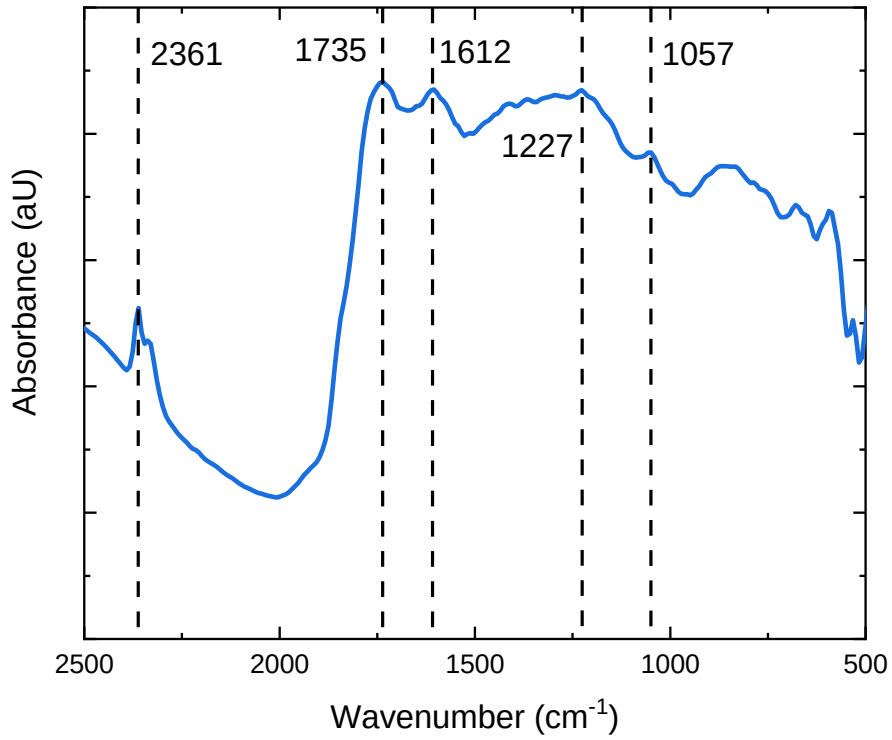

Figure 4. DRIFT-infrared spectra of Starbon®450-SO_3H.

N_2-physisorption – Py TPD

BET (Brunauer-Emmett-Teller) specific surface area, pore volume, xylose adsorption capacity and acid site density of Starbon®450-SO_3H are compiled in Table 2. Starbon®450-SO_3H shows a BET of 220 $m^2\ g^{-1}$, a pore volume of 0.4 $cm^3\ g^{-1}$ and a pore width of 3.9 nm, which are similar

to previously reported literature on similar materials.[39] As published in literature, a large surface area is preferable to facilitate the accessibility of xylose.[59]

Xylose adsorption was investigated to determine the availability of the reaction starting material xylose at the surface. Adsorption of sugar solutions (xylose[29, 60, 60] and fructose[61]) in aqueous phase onto solid materials has been investigated by previous researchers. According to Sairanen et al,[29] if the amount of xylose adsorbed on the catalyst surface is higher than the amount of acid sites, this indicates that xylose is adsorbed at sites other than the Brönsted sites as determined in our studies by pyridine titration. Brönsted acid sites are associated with direct dehydration of xylose into FUR, while Lewis acid sites are known to shift the equilibrium towards the isomers (especially xylulose).[9, 9, 62, 63, 63] Our results showed that the concentration of xylose adsorbed on the surface was slightly higher than the catalyst acid site density, suggesting that acid sites other than Brönsted are present on the surface of the catalyst. Nevertheless, even if Lewis acid sites were present on the surface of Starbon®450-SO_3H, they did not play a significant role in the isomerization of xylose into xylulose, since xylulose was not detected in HPLC. Other literature reported materials including mesoporous silica SBA-15 have been reported to have lower acid site densities (e.g. 0.16 mmol g^{-1}).[64]

Table 2. Textural properties (i.e., BET (A_{BET}), Pore volume (V_p) and Pore diameter (d_p) and acid properties of Starbon®450-SO_3H.

A_{BET} ($m^2\ g^{-1}$)	V_p ($cm^3\ g^{-1}$)	d_p (nm)	Xylose adsorption[a] (mmol g^{-1})	Acid site density[b] (mmol Py g^{-1})
220	0.4	3.9	0.32	0.29

[a] 50 mg of Starbon®450-SO_3H in 3 mL of a xylose solution (186 mmol l^{-1}). Agitation of the suspension for 24 h at room temperature (25 °C). Determination of xylose adsorption by HPLC analysis. Adsorbed amount of xylose per gram of catalyst.

[b] Pyridine (PY) titration value at 200 °C.

Monophasic system

Xylose dehydration into FUR in aqueous phase leads to rapid decomposition of FUR and provides low product yields[6]. As Figure S2 displays (in the Supplementary Information) the auto-catalyzed system of xylose dehydration (3 ml of a 186 mmol l^{-1} xylose solution) at 170 °C in various reaction times (1 – 6 h), the highest FUR yield was 38% at a xylose conversion of 58% (after 6 h). A selectivity to FUR (74%) was reached after 5 h, which decreased to 66% after 6 h. With the addition of Starbon®450-SO_3H (50 mg) to the aqueous xylose solution (3 ml of 186 mmol l^{-1}) at 170 °C in various reaction times (1-6 h), the highest FUR yield was 42% at a xylose conversion of 73% (after 6 h, Figure S2). When adding Starbon®450-SO_3H, FUR yield and xylose conversion increase in comparison to the auto-catalyzed system. This is due to the addition of acid sites into the system. In a similar published system, a high selectivity to FUR (67%) was reached after 2 h at 170 °C, which gradually decreased with increasing reaction time. Under similar conditions (2 h at 170 °C), alumina on cordierite reached a selectivity to FUR of 30%; polymeric resins, such as

Nafion NR40 and Amberlyst DT showed a selectivity to FUR of 48% and 27%, respectively.[6] In order to avoid FUR decomposition, and to increase its yield, a biphasic system was developed adding an organic solvent that would protect FUR formed.

Partition coefficient

The partitioning of FUR was investigated by conducting hydrothermal reactions wherein a solution of 5 wt% FUR in water was heated with CPME for 60 min at 170 °C at five different ratios of aqueous-to-organic solvent: 1:5, 1:2, 1:1, 2:1 and 5:1 (v/v) and 25 mg of Starbon®450-SO_3H. Figure S3 shows the FUR partition coefficients (P) obtained with CPME, where *P* was calculated using Eq. 6.[65]

$$P = \frac{[FUR]_{org}}{[FUR]_{aq}} \qquad \text{(Eq. 6)}$$

A FUR partition coefficient of 3.4 was obtained with an aqueous to CPME fraction ratio of 5:1. This value decreased to 3.3, 3.2, 3.0 and 2.8 as the aqueous-to-CPME fraction ratio increased to 1:2, 1:1, 2:1 and 5:1, respectively. The selection of the aqueous-to-organic phase ratio in a range of 1:5 to 5:1 has a rather low influence on the partition coefficient as highlighted in Fig. S3.

Effect of the Ratio Water-CPME on Furfural Yields

In order to evaluate the effect of the ratio water-CPME on catalyzed xylose conversion and furfural yields, eight ratios of aqueous to organic phase (5:0, 5:1, 3:1, 2:1, 1:1, 1:2, 1:3 and 1:5; v/v) were studied. When the reaction was performed in pure water (ratio 5:0), the yield of the produced FUR did not exceed 10%, and the selectivity was approximately 37% (Figure 1). Furthermore, the conversion of xylose was around 27%. By increasing the aqueous to organic phase ratio, the selectivity to FUR increased with values of 60%, 56%, 55% and 51% for water-CPME volumetric ratios of 5:1, 3:1, 2:1 and 1:1, respectively. Additionally, when the water-to-CPME volumetric

ratios increased even more to 1:3 and 1:5, the FUR yield increased to 18%, due to a concomitant increase of the conversion rate. Experiments employing pure CPME were excluded from this study, since xylose has been proven to be almost insoluble in this organic solvent, hence FUR yields are generally minimal.[66] Even though the selectivity and xylose conversion are higher at water-to-CPME volumetric ratios of 1:5 than at 1:3, it is not practical for industrial applications. Thus, the ratio of 1:3 was selected for further experiments. This is in accordance with published literature, since biphasic systems benefit from higher organic-to-aqueous phase ratios.[67]

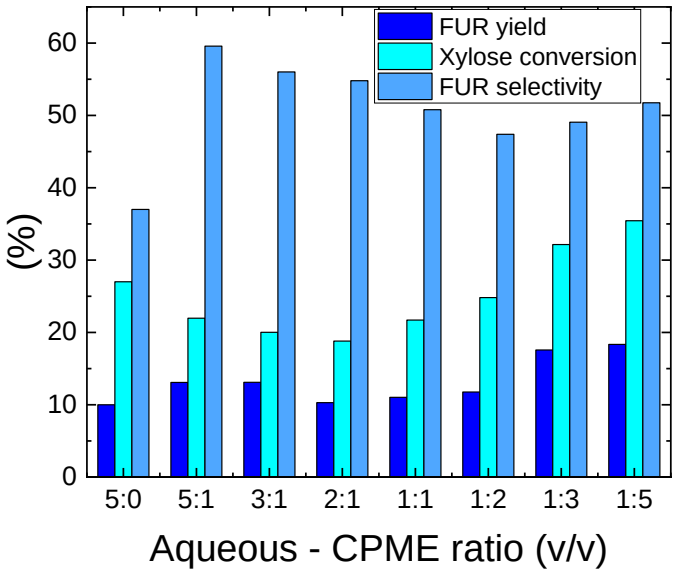

Figure 1. Effect of aqueous-to-organic ratio on FUR yield when using CPME. The effect was determined for a solution of xylose (186 mmol l^{-1}) heated for 60 min at 170 °C with 25 mg of Starbon®450-SO_3H (and then cooled down to 4 °C) at eight different ratios of aqueous to organic solvent: 5:0, 5:1, 3:1, 2:1, 1:1, 1:2, 1:3 and 1:5 (v/v).

Practically all xylose was converted at 200 °C in 1 h. Nevertheless, at 150 °C only 1.3% of the xylose was decomposed (Figure 2a). Yield of FUR varied from 0.7% to 69.5%. Based on the results, FUR yield increased when reaction temperature and reaction time increased, but decreased when reaction times longer than 17 h at 200 °C were used (Figure 2b). Selectivity to FUR ranged from 1.5% and 72.5%. Figure 2c shows that the highest selectivities were achieved

at low reaction temperatures (150 °C-170 °C) and long reaction times (>10 h) or short reaction times (1-10 h) and high temperatures (170 °C-200 °C).

Prediction models for xylose conversion, furfural yield and selectivity were also successfully determined based on the results. R^2 values indicated that the models explained 92-99% of variation in sample properties. The obtained models were then used to predict xylose conversion and FUR yield of the samples within the experimental design range. As illustrated in Figure 2, both reaction temperature and time were statistically significant for xylose conversion, FUR yield and selectivity. Interaction effects between reaction temperature and time were also significant based on the determined models. As an example, longer reaction times increased xylose conversion at lower temperatures, but the effect of time decreased at higher temperatures (Fig. 2a). Longer reaction times also decreased significantly FUR yield at higher temperatures (Fig. 2b). The highest selectivities were thus obtained by combining high reaction temperature with low reaction time, or low to medium reaction temperature with medium to high reaction time (Fig. 2c). The overlay plot in Fig. 2d also suggested that a local optimum, where both xylose conversion and FUR yield were maximized, existed within the experimental design range. Even though, another optimum could be found at reaction temperatures above 200 °C and reaction times below 6 h (Fig. 2d), these conditions were not possible to perform in the present set-up. Furthermore, those experimental conditions could present a challenge for the hydrothermal stability of the catalyst. A verification experiment was thus performed by combining a reaction temperature of 175 °C with a reaction time of 18 hours. The obtained results indicated that 100% of xylose was converted to 69.3% FUR during the first cycle. The verification results were in good agreement with the model predictions, which suggested that 101 ± 25.0% of xylose would be converted to 66.9 ± 10.5% (α=0.10). The results of analysis of variance are summarised in tables S1, S2 and S3 (in the Supplementary Information), for FUR yield, xylose conversion and selectivity to FUR, respectively.

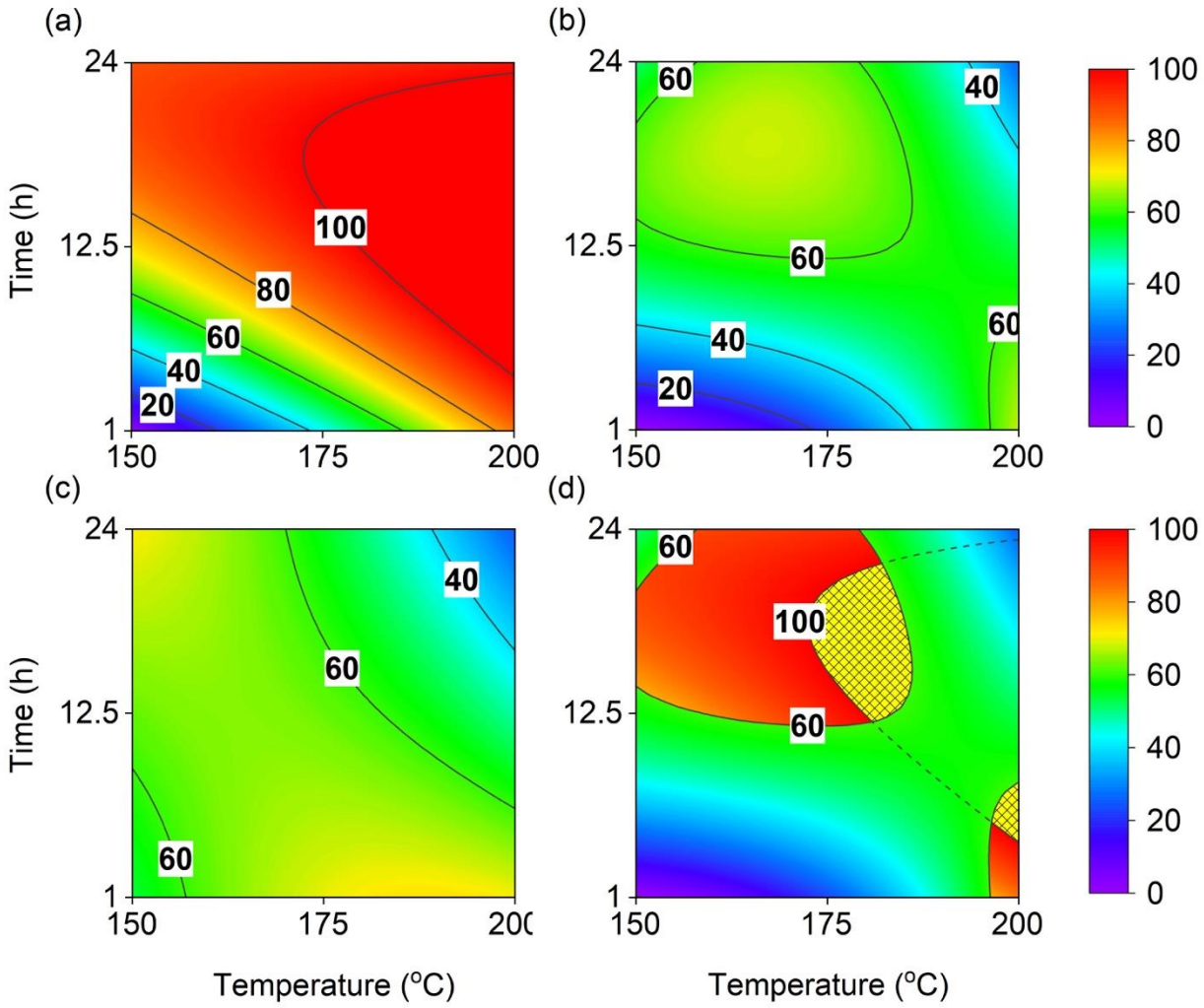

Figure 2. Contour plots based on model prediction for (a) conversion of xylose (%, R^2 = 0.92); (b) furfural yield (%, R^2 = 0.99); selectivity (%, R^2 = 0.92), and; (c) an overplay plot of xylose conversion and furfural yield. The yellow patterned area in (d) indicates 100% xylose conversion and a furfural yield of >60% based on the model predictions.

Reusability

The hydrothermal stability of Starbon®450-SO_3H under the investigated reaction conditions was tested by employing the same catalyst in a series of xylose dehydration reactions. Prior to each cycle, the sample was washed with deionized water and dried at 105 °C. Figure 5 shows three

consecutive reaction runs of Starbon®450-SO_3H (at 175 °C in 18 h using 21 mg of Starbon®450-SO_3H in 0.75 ml of xylose concentration 186 mmol l^{-1} and 2.25 ml of CPME). The notation for Starbon®450-SO_3H after the reusability test includes a hyphen and the reusability cycle number, e.g. Starbon®450-SO_3H_{-1}.

After 3 cycles, the catalytic activity of the reused catalyst stayed stable, yielding 70% FUR at complete xylose conversion. Under similar conditions (175 °C, 18 h and 1:3 aqueous to CPME phase ratio), the auto-catalyzed system reaches 100% xylose conversion and 59% FUR yield.

As a non-destructive method, Raman spectroscopy is commonly used to characterize the structure of carbon-based materials. As shown in Figure 6**,** all the samples show two pronounced bands: D and G bands at around 1344 cm^{-1} and 1593 cm^{-1}, respectively, which are a typical characteristic for graphitic carbon and show the presence of aromatic carbon sheets.[68] The D-band is associated with the breathing modes of sp^3 atoms and is activated only in the presence of defects and disorder in the carbon structure, whilst the G-band is attributed to the vibrations of sp^2 bonded carbon atoms in the hexagonal lattice. The higher frequency position of the G-band and the broad and intense D-band indicate the presence of amorphous phase.[68]

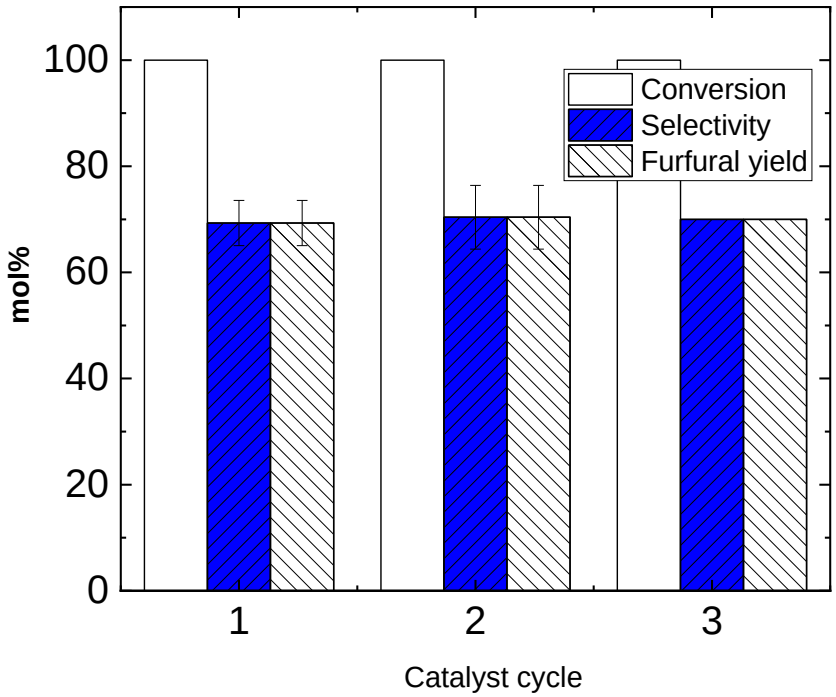

Figure 5. Reusability of Starbon®450-SO_3H for the dehydration of xylose to FUR using 21 mg of catalyst at 175 °C for 18 h (xylose conversion (white bar), FUR yield (blue bar) and selectivity to FUR (striped bar)).

As shown in Figure 6, the Raman spectra of the catalyst before and after the cycles are very similar. The intensity ratio of the G and D band, I_D/I_G can be used to estimate the defect level. The I_D/I_G ratios are virtually identical: 0.984, 0.961, 0.962 and 0.964 for Starbon®450-SO_3H_{-fresh}, Starbon®450-SO_3H_{-1}, Starbon®450-SO_3H_{-2} and Starbon®450-SO_3H_{-3}, respectively. Therefore, the catalyst is stable and reusable, in agreement with the reusability tests which also did not show any loss of yield and selectivity between the three cycles.

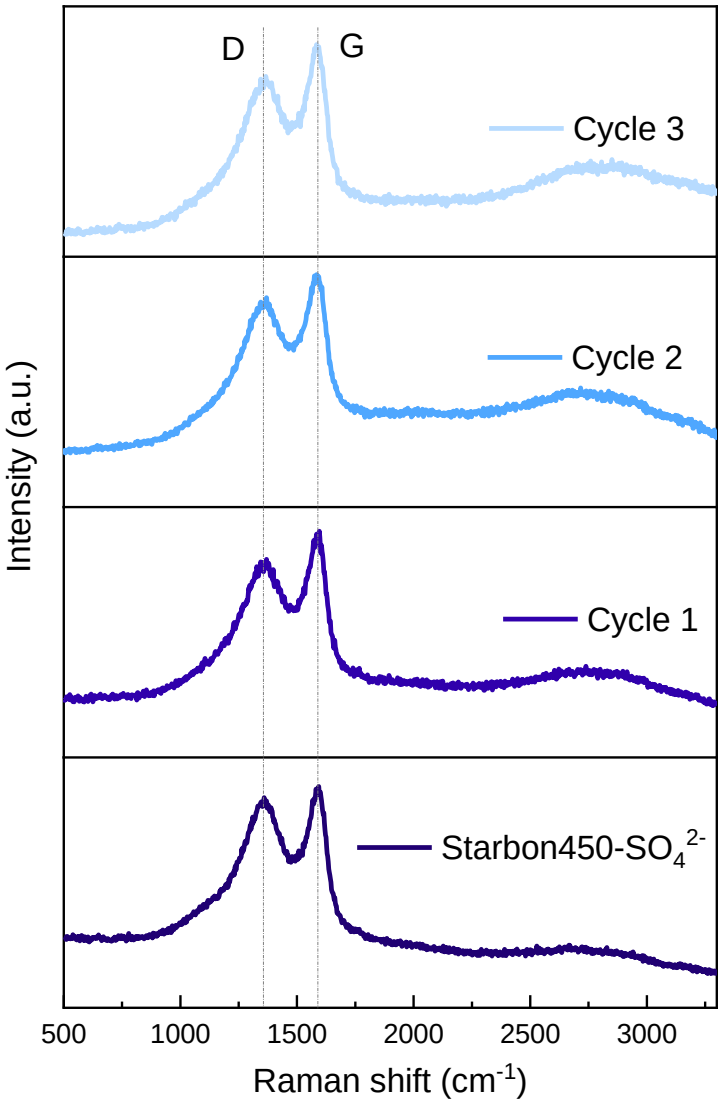

Figure 6. Raman spectra of the catalyst before and after reusability cycles.

Apart from Raman spectra studies, a detailed XPS analysis was performed to get a deeper insight about the surface composition of the materials. In Fig. S5 and Table S3 (In the Supplementary Information) the binding energy values and surface atomic composition of metal oxides before and after hydrothermal reaction are shown. As it can be demonstrated, there are no significant changes in the chemical composition of the surface of Starbon®450-SO_3H before and after hydrothermal reaction.

Starbon®450-SO_3H is a very attractive solid acid catalyst to form FUR from xylose due to its high BET surface area, excellent hydrothermal stability, and high acid site density. It is interesting to compare its performance with those of other carbon-based catalysts employed in similar set-ups.

Wang et al developed a Miscanthus-based catalyst with sulfonic groups for the FUR formation from xylose and xylan in a CPME/H_2O 3:1 phase ratio (v/v). Under optimized conditions, they reported a FUR yield of 60% and 42% from xylose and xylan, respectively (190 °C in 1 h).[69] A sulfated lignin-based catalyst was developed by Antonyraj and Haridas to form FUR and hydroxymethylfurfural (HMF) from xylose and fructose, respectively, in a methyl isobutyl ketone (MIBK)/H_2O 7:3 phase ratio (v/v) system. They reported yields of up to 65% FUR at 175 °C in 3 h from xylose and 27% HMF at 150 °C in 3 h from fructose.[70]

In this work, we have shown how statistical methods can support the design of experiments. Furthermore, Starbon® can be functionalized with sulfuric acid and efficiently form FUR from xylose. Starbon®450-SO_3H has shown hydrothermal stability under the experimental conditions presented in this paper and it has reached higher FUR yields in comparison to similar systems using carbonaceous catalysts. Moreover, it can be easily separated from the reaction media and further reused without losing its catalytic activity.

A possible alternative to reduce the reaction time presented in this study, could be to increase the reaction temperature around 200 °C. As Fig. 2 shows, an area with FUR yields above 60% can be reached at approximately 200 °C under 6 h. Naturally, hydrothermal stability of Starbon®450-SO_3H and its feasible reuse under similar experimental conditions have to be investigated. An interesting option to avoid further FUR decomposition would be to modify the batch system for a plug-flow reactor with an optimized residence time.

Conclusions

Furfural formation from xylose in the presence of Starbon®450-SO_3H was studied in a biphasic system using CPME as organic solvent. The major product of the catalyzed dehydration reaction of xylose was FUR when adding Starbon®450-SO_3H. Minor products detected in the system were carboxylic acids and decomposition products, such as humins. The maximum mole fraction yield obtained was 70% in 18 h at 175 °C at complete xylose conversion. Whereas the auto-catalyzed system at same conditions yielded 59% FUR. Starbon®450-SO_3H showed a high selectivity to FUR in both the monophasic and biphasic systems. Under these experimental conditions, it is demonstrated that the reusability potential of the carbon-based mesoporous material is possible without decreasing its catalytic activity.

Acknowledgements

This research has been done in collaboration with Stora Enso and funded through Erasmus Mundus Joint Doctoral Programme SELECT+, the support of which is gratefully acknowledged. GGM acknowledges the support of COST Action FP1306 to embark upon a Short-Term Scientific Mission at Universidad de Cordoba. The authors are also grateful for the support of the staff at the Department of Bioproducts and Biosystems at Aalto University, especially to Josphat Phiri for the Raman studies; and Hans Orassaari; and at Universidad de Cordoba in the Nanoscale Chemistry and Biomass/Waste Valorisation group, especially to Antonio Pineda. This work made use of Aalto University Bioeconomy Facilities. The publication was prepared with support from RUDN University Program 5-100. JL is a Serra Húnter Fellow and is grateful to ICREA Academia program and grant GC 2017 SGR 128.

References

[1] S. Peleteiro, S. Rivas, J. L. Alonso, V. Santos and J. C. Parajó. *Bioresour. Technol.* **2016,** *202,* 181-191.

[2] K. J. Zeitsch. *14. Applications of furfural, 13,* (Eds.: K. J. Zeitsch.) Elsevier B.V., **2000,** pp. 98-103.

[3] S. J. Canhaci, R. F. Perez, L. E. P. Borges and M. A. Fraga. *Appl. Catal. , B.* **2017,** *207,* 279-285.

[4] Y. Luo, Z. Li, X. Li, X. Liu, J. Fan, J. H. Clark and C. Hu. *Catal. Today.* **2019,** *319,* 14-24.

[5] A. S. Mamman, J. Lee, Y. Kim, I. T. Hwang, N. Park, Y. K. Hwang, J. Chang and J. Hwang. *Biofuels, Bioprod. Biorefin.* **2008,** *2,* 438-454.

[6] G. Gómez Millán, Z. El Assal, K. Nieminen, S. Hellsten, J. Llorca and H. Sixta. *Fuel Process Technol.* **2018,** *182,* 56-67.

[7] A. S. Dias, S. Lima, M. Pillinger and A. A. Valente. *Catal. Lett.* **2007,** *114,* 151-160.

[8] H. Li, A. Deng, J. Ren, C. Liu, W. Wang, F. Peng and R. Sun. *Catal. Today.* **2014,** *234,* 251-256.

[9] R. Weingarten, G. A. Tompsett, W. C. Conner Jr. and G. W. Huber. *J. Catal.* **2011,** *279,* 174-182.

[10] S. J. You, Y. T. Kim and E. D. Park. *Reaction Kinetics, Mechanisms and Catalysis.* **2014,** *111,* 521-534.

[11] C. Moreau, R. Durand, D. Peyron, J. Duhamet and P. Rivalier. *Ind. Crops Prod.* **1998,** *7,* 95-99.

[12] R. O'Neill, M. N. Ahmad, L. Vanoye and F. Aiouache. *Ind Eng Chem Res.* **2009,** *48,* 4300-4306.

[13] R. Sahu and P. L. Dhepe. *ChemSusChem.* **2012,** *5,* 751-761.

[14] S. Lima, A. Fernandes, M. M. Antunes, M. Pillinger, F. Ribeiro and A. A. Valente. *Catal. Lett.* **2010,** *135,* 41-47.

[15] E. I. Gürbüz, J. M. R. Gallo, D. M. Alonso, S. G. Wettstein, W. Y. Lim and J. A. Dumesic. *Angewandte Chemie International Edition.* **2013,** *52,* 1270-1274.

[16] L. R. Ferreira, S. Lima, P. Neves, M. M. Antunes, S. M. Rocha, M. Pillinger, I. Portugal and A. A. Valente. *Chem. Eng. J.* **2013,** *215–216,* 772-783.

[17] A. Yepez, A. Garcia, M. S. Climent, A. A. Romero and R. Luque. *Catal. Sci. Technol.* **2014,** *4,* 428-434.

[18] M. J. C. Molina, M. L. Granados, A. Gervasini and P. Carniti. *Catal. Today.* **2015,** *254,* 90-98.

[19] G. H. Jeong, E. G. Kim, S. B. Kim, E. D. Park and S. W. Kim. *Microporous Mesoporous Mater.* **2011,** *144,* 134-139.

[20] I. Agirrezabal-Telleria, J. Requies, M. B. Güemez and P. L. Arias. *Appl. Catal. , B.* **2012,** *115–116,* 169-178.

[21] I. Agirrezabal-Telleria, C. García-Sancho, P. Maireles-Torres and P. L. Arias. *Chin. J. Catal.* **2013,** *34,* 1402-1406.

[22] I. Agirrezabal-Telleria, J. Requies, M. B. Güemez and P. L. Arias. *Appl. Catal. , B.* **2014,** *145,* 34-42.

[23] P. Bhaumik, T. Kane and P. L. Dhepe. *Catal. Sci. Technol.* **2014,** *4,* 2904-2907.

[24] A. S. Dias, M. Pillinger and A. A. Valente. *J. Catal.* **2005,** *229,* 414-423.

[25] S. Kaiprommarat, S. Kongparakul, P. Reubroycharoen, G. Guan and C. Samart. *Fuel.* **2016,** *174,* 189-196.

[26] E. Lam, J. H. Chong, E. Majid, Y. Liu, S. Hrapovic, A. C. W. Leung and J. H. T. Luong. *Carbon.* **2012,** *50,* 1033-1043.

[27] A. S. Dias, M. Pillinger and A. A. Valente. *Appl. Catal. , A.* **2005,** *285,* 126-131.

[28] A. S. Dias, M. Pillinger and A. A. Valente. *Microporous Mesoporous Mater.* **2006,** *94,* 214-225.

[29] E. Sairanen, K. Vilonen, R. Karinen and J. Lehtonen. *Top. Catal.* **2013,** *56,* 512-521.

[30] E. Lam, E. Majid, A. C. W. Leung, J. H. Chong, K. A. Mahmoud and J. H. T. Luong. *ChemSusChem.* **2011,** *4,* 535-541.

[31] I. Agirrezabal-Telleria, A. Larreategui, J. Requies, M. B. Güemez and P. L. Arias. *Bioresour. Technol.* **2011,** *102,* 7478-7485.

[32] C. Sener, A. H. Motagamwala, D. M. Alonso and J. A. Dumesic. *ChemSusChem.* **2018,** *11,* 2321.

[33] H. Xiong, H. N. Pham and A. K. Datye. *Green Chem.* **2014,** *16,* 4627-4643.

[34] C. Termvidchakorn, V. Itthibenchapong, S. Songtawee, B. Chamnankid, S. Namuangruk, K. Faungnawakij, T. Charinpanitkul, R. Khunchit, N. Hansupaluk, et al. *Advances in Natural Sciences: Nanoscience and Nanotechnology.* **2017,** *8,* 035006.

[35] R. Jalili, D. Esrafilzadeh, S. H. Aboutalebi, Y. M. Sabri, A. E. Kandjani, S. K. Bhargava, E. Della Gaspera, T. R. Gengenbach, A. Walker, et al. *Nature Communications.* **2018,** *9,* 5070.

[36] V. L. Budarin, J. H. Clark, R. Luque, D. J. Macquarrie, A. Koutinas and C. Webb. *Green Chem.* **2007,** *9,* 992-995.

[37] V. Budarin, R. Luque, D. J. Macquarrie and J. Clark. *Chemistry A European Journal.* **2007,** *13,* 6914-6919.

[38] V. L. Budarin, J. H. Clark, R. Luque and D. J. Macquarrie. *Chem. Commun.* **2007,** 634-636.

[39] J. H. Clark, V. Budarin, T. Dugmore, R. Luque, D. J. Macquarrie and V. Strelko. *Catal. Commun.* **2008,** *9,* 1709-1714.

[40] V. Budarin, J. H. Clark, J. J. E. Hardy, R. Luque, K. Milkowski, S. J. Tavener and A. J. Wilson. *Angew. Chem. Int. Ed.* **2006,** *45,* 3782-3786.

[41] K. Watanabe. *Molecules.* **2013,** *18,*

[42] G. Gómez Millán, S. Hellsten, A. W. T. King, J. Pokki, J. Llorca and H. Sixta. *J. Ind. Eng. Chem.* **2019,** *72,* 354-363.

[43] K. Lamminpää, J. Ahola and J. Tanskanen. *Ind Eng Chem Res.* **2012,** *51,* 6297-6303.

[44] K. Dussan, B. Girisuta, M. Lopes, J. J. Leahy and M. H. B. Hayes. *ChemSusChem.* **2016,** *9,* 492-504.

[45] S. Givry, C. Bliard and F. Duchiron. *Carbohydr. Res.* **2007,** *342,* 859-864.

[46] M. Ojeda, A. M. Balu, A. A. Romero, P. Esquinazi, J. Ruokolainen, H. Sixta and R. Luque. *ChemCatChem.* **2014,** *6,* 2847-2853.

[47] S. Brunauer, P. H. Emmett and E. Teller. *Journal of the American Chemical Society.* **1938,** *35,* 309.

[48] E. P. Barrett, L. G. Joyner and P. P. Halenda. *Journal of the American Chemical Society.* **1951,** *73,* 373.

[49] A. Pineda, A. M. Balu, J. M. Campelo, R. Luque, A. A. Romero and J. C. Serrano-Ruiz. *Catalysis Today.* **2012,** *187,* 65-69.

[50] C. Pirola, I. Rossetti and V. Ragaini. *La Chimica & L'Industria.* **2013,** *2,* 136-145.

[51] R. Leardi. *Analytica Chimica Acta.* **2009,** *652,* 161-172.

[52] A. Aldana-Pérez, L. Lartundo-Rojas, R. Gómez and M. E. Niño-Gómez. *Fuel.* **2012,** *100,* 128-138.

[53] M. Baikousi, Y. Georgiou, C. Daikopoulos, A. B. Bourlinos, J. Filip, et al. *Carbon.* **2015,** *93,* 636-647.

[54] C. J. Mena Duran. **2014,**

[55] J. C. Yang, M. J. Jablonsky and J. W. Mays. *Polymer.* **2002,** *43,* 5125-5132.

[56] G. Chen and B. Fang. *Bioresour. Technol.* **2011,** *102,* 2635-2640.

[57] E. Damian Risberg, L. Eriksson, J. Mink, L. G. M. Pettersson, M. Y. Skripkin and M. Sandström. *Inorg. Chem.* **2007,** *46,* 8332-8348.

[58] A. Thamri, H. Baccar, C. Struzzi, C. Bittencourt, A. Abdelghani and E. Llobet. *Scientific Reports.* **2016,** *6,* 35130.

[59] R. Karinen, K. Vilonen and M. Niemelä. *ChemSusChem.* **2011,** *4,* 1002-1016.

[60] R. Ranjan, S. Thust, C. E. Gounaris, M. Woo, C. A. Floudas, M. v. Keitz, K. J. Valentas, J. Wei and M. Tsapatsis. *Microporous Mesoporous Mater.* **2009,** *122,* 143-148.

[61] V. V. Ordomsky, J. van der Schaaf, J. C. Schouten and T. A. Nijhuis. *ChemSusChem.* **2012,** *5,* 1812-1819.

[62] V. Choudhary, S. I. Sandler and D. G. Vlachos. *ACS Catal.* **2012,** *2,* 2022-2028.

[63] J. Iglesias, J. A. Melero, G. Morales, M. Paniagua and B. Hernández. *ChemCatChem.* **2016,** *8,* 2089-2099.

[64] M. J. Gracia-Trujillo, M. J. Jurado-Pescuezo, M. D. Gracia-Serrano, J. M. Campelo, D. Luna, J. M. Marinas and A. A. Romero. *Stud. Surf. Sci. Catal.* **2008,** *174,* 1331-1334.

[65] A. Mittal, S. K. Black, T. B. Vinzant, M. O'Brien, M. P. Tucker and D. K. Johnson. *ACS Sustainable Chem. Eng.* **2017,**

[66] S. Le Guenic, D. Gergela, C. Ceballos, F. Delbecq and C. Len. *Molecules.* **2016,** *21,*

[67] J. E. Romo, N. V. Bollar, C. J. Zimmermann and S. G. Wettstein. *ChemCatChem.* **2018,** *10,* 4805-4816.

[68] A. C. Ferrari and J. Robertson. *Phys. Rev. B.* **2000,** *61,* 14095-14107.

[69] Y. Wang, F. Delbecq, W. Kwapinski and C. Len. *Molecular Catalysis.* **2017,** *438,* 167-172.

[70] C. A. Antonyraj and A. Haridas. *Catalysis Communications.* **2018,** *104,* 101-105.